Astronomy & Astrophysics manuscript no. article
(DOI: will be inserted by hand later)
April 24, 2007

Dust Distribution during Reionization

Erik Elfgren[1], François-Xavier Désert[2], Bruno Guiderdoni[3], and Eric Hivon[4]

[1] Department of Physics, Luleå University of Technology, SE-971 87 Luleå, Sweden
[2] Laboratoire d'Astrophysique, Observatoire de Grenoble, BP 53, 414 rue de la piscine, 38041 Grenoble Cedex 9, France
[3] Universit Lyon 1, Centre de Recherche, Astrophysique de Lyon, Observatoire de Lyon, 9 avenue Charles Andr, 69230 Saint Genis Laval ; CNRS, UMR 5574.
[4] IPAC/Caltech, Mail Code 100-22, 770 S. Wilson Av., Pasadena, CA 91125, USA

Received ¡date¿ / Accepted ¡date¿

Abstract. The dust produced by the first generation of stars will be a foreground to Cosmic Microwave Background. In order to evaluate the effect of this early dust, we calculate the power spectrum of the dust emission anisotropies and compare it with the sensitivity limit of the Planck satellite.
The spatial distribution of the dust is estimated through the distribution of dark matter. At small angular scales ($\ell \gtrsim 1000$) the dust signal is found to be noticeable for certain values of dust lifetime and dust production rates. The dust signal is also compared to sensitivities of other instruments. The early dust emission anisotropies are also compared to those of local dust and found to be similar in magnitude at mm wavelength.

Key words. Dust – CMB – Reionization – Power spectrum

1. Introduction

The importance of the Cosmic Microwave Background (CMB) as a cosmological tool has been demonstrated thoroughly during the last few years. It has been used to evaluate the age of the universe, the Hubble parameter, the baryon content, the flatness and the optical depth of the reionization, Bennett et al. (2003). It has also been used to set upper limits on the non-Gaussianity of the primary fluctuations, Komatsu et al. (2003); the Sunyaev-Zeldovich fluctuations from the first stars, Oh et al. (2003); the primordial magnetic fields, Subramanian et al. (2003); the spatial curvature of the universe, Efstathiou (2003); the formation of population III stars, Cen (2003); and the neutrino masses, Hannestad (2003).

However, in order to interpret the CMB signal correctly, its foregrounds must also be well known.

In this paper we focus on one particular aspect of the foregrounds of the CMB: the dust from the first generation of stars. It is here assumed that dust was created during the reionization period in the first generation of stars and was then ejected into the intergalactic medium (IGM). The dust is heated by the ionizing photons to a temperature slightly above T_{CMB}. The net effect on the CMB is a small monopole distortion of the CMB with a characteristic electromagnetic spectrum close to the CMB primary anisotropy (ΔT) spectrum times the frequency squared. This effect of the dust on the CMB was studied in Elfgren & Désert (2004).

Send offprint requests to: Erik Elfgren, e-mail: elf@ludd.luth.se

Moreover, the dust will also have a characteristic spatial distribution which could be used to identify its signal. The distribution will give rise to anisotropies in the dust emission which can be measured with several current and future experiments. The objective of this paper is to determine this spatial distribution and its resulting anisotropies.Of particular interest is the Planck satellite mission, but also other instruments, like ALMA, SCUBA, MAMBO and BLAST could be of interest.

The spatial distribution of the dust is estimated with help of GalICS (Galaxies In Cosmological Simulations) N-body simulations of dark matter Hatton et al. (2003), which are described in more detail in section 2. The dust distribution is then combined with the intensity of the dust emission, and this is integrated along the line of sight. The resulting angular power spectrum is then computed as C_ℓ and compared with detection limits of Planck.

In the following, we assume a ΛCDM universe with $\Omega_{tot} = \Omega_m + \Omega_\Lambda = 1$, where $\Omega_m = \Omega_b + \Omega_{DM} = 0.133/h^2$, $\Omega_b = 0.0226/h^2$, $h = 0.72$ and $\tau_e = 0.12$ as advocated by WMAP, Spergel et al. (2003), using WMAP data in combination with other CMB datasets and large scale structure observations (2dFGRS + Lyman α).

2. Dark Matter Simulations

The distribution of dark matter in the universe is calculated using the GalICS program. The cosmological N-body simulation we refer to throughout this paper is done using

the parallel tree-code developed by Ninin (1999). The power spectrum is set in agreement with Eke et al. (1996): $\sigma_8 = 0.88$, and the Dark Matter (DM) density field was calculated from z=35.59 to z=0, outputting 100 snapshots spaced logarithmically in the expansion factor.

GalICS is a hybrid model for hierarchical galaxy formation studies, combining the outputs of large cosmological N-body simulations with simple, semi-analytic recipes to describe the fate of the baryons within dark matter halos. The simulations produce a detailed merging tree for the dark matter halos, including complete knowledge of the statistical properties arising from the gravitational forces.

The basic principle of the simulations is to randomly distribute a number of dark matter particles N^3 with mass $M_{\rm DM}$ in a box of size L^3. Then, as time passes, the particles interact gravitationally, clumping together and forming structures. The clumps of Dark Matter are called halos and in our simulation we require at least 5 particles to clump together before we call it a halo. There are supposed to be no other forces present than the gravitation and the boundary conditions are assumed to be periodic.

In the simulations we used the side of the box of the simulation is $L = 100h^{-1}$ Mpc and the number of particles are 256^3 which implies a particle mass of $\sim 5.51 \times 10^9 h^{-1} M_\odot$. Furthermore, for the simulation of Dark Matter, the cosmological parameters were $\Omega_\Lambda = 2/3$, $\Omega_m = 1/3$ and $h = 2/3$. The simulations of the Dark Matter were done before the results from WMAP were published which explains the difference between these parameters and the values used elsewhere in this paper, as stated in the instroduction. Fortunately, the temporal distribution of the dust is independent of the value of h which means that the impact of this small discrepancy is not very important. Between the assumed initial dust formation at $z \sim 15$ and the end of this epoch in the universe at $z \sim 5$, there are 51 snapshots. In each snapshot a friend-of-friend algorithm was used to identify virialized groups of at least five DM particles. This number of required particles means that the first halos in our model formed at $z = 14.7$.

In order to make a correct large-scale prediction of the distribution of the Dark Matter and therefore the dust, the size of the box would have to be of Hubble size, i.e. $\sim 3000h^{-1}$ Mpc. However, for a given simulation time, increasing the size of the box and maintaining the same number of particles would mean that we loose in mass resolution, which is not acceptable if we want to reproduce a fairly realistic scenario of the evolution of the universe.

There is another way to achieve the desired size of the simulation without loosing in detail or making huge simulations. This method is called MoMaF (Mock Map Facility) and is described in detail in Blaizot et al. (2005). The basic principle is to use the same box, but at different stages in time and thus a cone of the line of sight can be established. In order to avoid replication effects, the periodic box is randomly rotated for each time-step. This means that there will be loss of correlation information on the edges of the box, since those parts will be gravitationally disconnected from the adjacent box. Fortunately, this loss will only be of the order of 10% as shown in Blaizot et al. (2005). For scales larger than the size of the box, there is obviously no information whatsoever on correlation from the simulation

2.1. Validity of Simulation

The distribution of galaxies resulting from this GalICS simulation has been compared with the 2dS Colless et al. (2001) and the Sloan Digital Sky Survey Szapudi et al. (2001) and found to be realistic on the angular scales of $3' \lesssim \theta \lesssim 30'$, see Blaizot et al. (2006). The discrepancy in the spatial correlation function for other values of θ can be explained by the limits of the numerical simulation. Obviously, any information on scales larger than the size of the box ($\sim$ 45') is not reliable. Fortunately, the dust correlations increase at smaller angles while the CMB and many other signals decrease. This means that our lack of information on angular scales $\theta > 45'$ ($\ell \lesssim 250$) will not be important, as can be seen in Fig. 4. The model has also proven to give reasonable results for Lyman Break Galaxies at $z = 3$, IBlaizot et al. (2004). It is also possible to model Active Galactic Nuclei using the same model, Cattaneo et al. (2005).

Since it is possible to reproduce reasonable correlations from semi-analytic modelling of galaxy formation within this simulation at $z = 0 - 3$, we hereafter attempt to do so at higher z when the early dust is produced.

3. Model

Since very little is known about the actual distribution of the dust throughout the universe at this time, we simply assume that the dust distribution follows the dark matter distribution. We propose two different ways for this to happen and explore these. The first is to let the dust be proportional to the dark matter halos, the second is to make a hydrodynamical smoothing of the dark matter density field and set the dust density proportional to this density. In both cases we assume that

$$\rho_{dust}(\boldsymbol{r}, z) \propto \rho_{DM}(\boldsymbol{r}, z), \tag{1}$$

where ρ_{DM} represents either the Halo method or the Smoothing method density. We will focus on the Halo method since the dust was created in galaxies which are found in the halos. The dust will propagate to some extent but, for simplicity, we assume that it stays close to the Dark Matter halo. The hydrodynamical smoothing case is included for reference only.

In order to estimate the measured intensity, we need to calculate this distribution in terms of the intensity from the dust emission. The early dust is optically thin and its intensity as a function of redshift has been calculated in Elfgren & Désert (2004) and is shown in Fig. 1. This model assumes that the fraction of metals produced in stars that end up as dust are $f_d = 0.3$. The mean dust life-time is a largly unknown parameter and therefore three different values are explored, $\Delta t = 0.1, 1, 10$ Gyr.

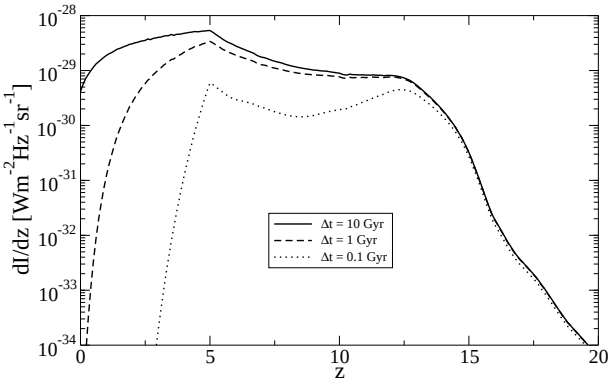

Fig. 1. Intensity contribution from the dust per time-step z integrated over all frequencies. This model assumes that the fraction of metals produced in stars that end up as dust are f_d = 0.3. The mean dust life-time is a largly unknown parameter and therefore three different values are explored, Δt = 0.1, 1, 10 Gyr.

In our present model, we put the spatial distribution of the dust intensity to

$$\frac{dI}{dz}(\boldsymbol{r}, z) = \frac{dI(z)}{dz} \cdot \frac{\rho_{DM}(\boldsymbol{r}, z)}{\langle \rho_{DM} \rangle (z)}. \quad (2)$$

where $dI(z)/dz$ is the dust intensity at redshift z as measured at $z = 0$ and $\langle \rho_{DM} \rangle (z)$ is the mean Dark Matter density at redshift z. The MoMaF method (see section 2) is then used to project the emitted intensity from the dust on a 45'×45' patch along the line of sight. The contribution from each simulated box is added and the integrated dust intensity is calculated.

For $z > 2.3$, the time-steps are smaller than the size of the box and each box overlap with the next box along the line of sight. However, for $z < 2.3$ the time-steps were simulated too far apart and when we pile the boxes, there will be a small part of the line of sight that will not be covered. Fortunately, this is of little consequence since the dust intensity is low at this time and the gap is small. Each box (45'×45') is divided into a grid according to the resolution that we wish to test. For Planck this means a grid that is 18×18 pixels, for SCUBA 45×45 pixels.

To check the normalization of the resulting intensity image, we have calculated its $\sum dI_{x,y}/N^2_{pix}$, where $dI_{x,y}$ is the observed intensity on pixel x, y and N^2_{pix} is the number of pixels, and found it to be equal to $\int dI(z)dz$ to within a few per cent.

4. Results and Discussion

As described above, the MoMaF technique produces an image of the line of sight. This image represents the patch of the sky covered by the box, 150 co-moving Mpc^2 which translates to $\sim$ 45 arcmin^2 at z = 14.7. In order to avoid artifacts on the edges, the image is apodized, whereafter the image is Fourier transformed into frequency space P_k. In order to convert this spectrum into spherical harmonics correlation function we apply the following transformation:

$$\ell = k2\pi/\theta, \quad (3)$$

$$C_\ell = \theta^2 C_k, \quad (4)$$

where θ is the size in radians of the box being analyzed. These C_ℓ are then calculated at a frequency ν = 353 GHz, which is one of the nine Planck frequency channels. As found in Elfgren & Désert (2004), the intensity is proportional to the frequency squared which means that the power spectrum (expressed in CMB thermodynamic units) from the dust at a frequency ν will be

$$C_\ell(\nu) = C_\ell(353\ \mathrm{GHz}) \cdot \left(\frac{\nu}{353\ \mathrm{GHz}}\right)^4. \quad (5)$$

if C_ℓ is given in terms of μK(CMB). In order to estimate an average power spectrum, 400 such images were generated and the C_ℓ were averaged of these. For comparison, we also tried to paste all these images together and calculate the C_ℓ for this (180×180 pixels) image. The result was very similar to the average C_ℓ. To validate our results, we have also calculated the variance of the images and compared with $\sum_\ell \frac{2\ell+1}{4\pi} C_\ell$ and found them to be compatible. The resulting power spectra can be seen in Fig. 2. The lifetime of these dust particles is a largely unknown factor and we plot three different lifetimes, 0.1, 1, 10 Gyrs (for a more detailed discussion on dust lifetimes, see Draine (1990)). Furthermore, the dust intensity is proportional to the fraction of the formed metals that actually end up as dust, which we have assumed to be f_d = 0.3. This means that the dust power spectrum is

$$C_\ell(f_d) = C_\ell(f_d = 0.3) \cdot (f_d/0.3)^2. \quad (6)$$

We note that there is only a small difference between dust lifetimes of 10 Gyrs and 1 Gyr, while the 0.1 Gyr is lower by a factor four. The lowest curve in the figure represents the hydrodynamical smoothing method of distributing the dust for a dust lifetime of 1 Gyr. Naturally, it is significantly lower than the corresponding C_ℓ for the Halo method since the DM halos are much more grainy (especially early in the history) than the smoothed DM field. The difference between the two methods is a factor of $\sim$ 10 but they do not have exactly the same form.

The dust frequency spectrum will be distinctly different from that of other sources in the same frequency range. In Fig. 3, we compare this spectrum with that of the primoridal CMB ΔT anisotropies and that of galactic dust, T=17 K, Boulanger et al. (1996). In order to focus on the forms of the spectra, we normalize the three curves to one at ν = 353 GHz. In case of a weak early dust signal, this frequency signature could help us identify the signal by component separation spectral methods.

4.1. Detection with Planck?

The Planck satellite[1], due for launch in 2007, will have an angular resolution ranging from 30'−5' and will cover the whole sky.

[1] Homepage: http://www.rssd.esa.int/index.php?project=Planck

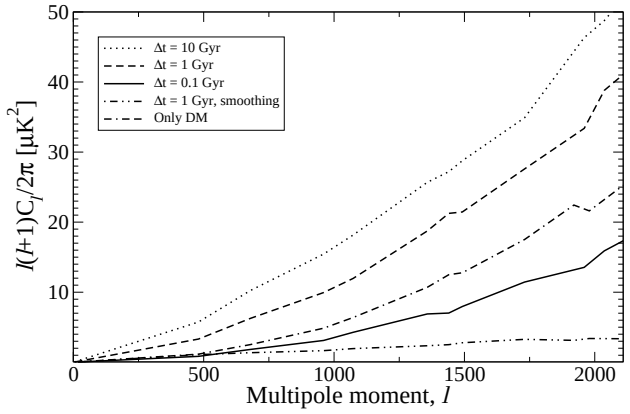

Fig. 2. Dust power spectrum in CMB thermodynamic units at 353 GHz for a map 45'×45' and Planck resolution 5' for three different lifetimes for the dust particles, 0.1, 1, 10 Gyrs, with a solid, dashed and dotted line respectively. The DM smoothing method for a dust lifetime of 1 Gyr is the dot-dot-dash line. We note that the DM smoothing method gives correlations that are approximately a factor ten lower than the DM halo method. Also, the form is not quite the same.

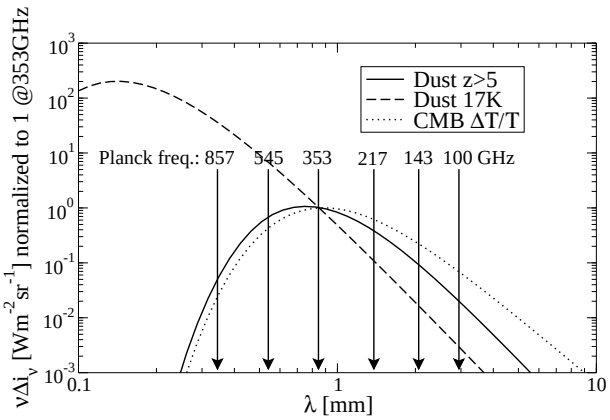

Fig. 3. The form of the early dust spectrum compared to the form of galactic dust (with a temperature of 17K) and the CMB along with indicators of the Planck HFI frequencies. The curves have been normalized to 1 at 353 GHz. We see that the early dust has a special spectral signature.

The Planck High Frequency Instrument will measure the submillimetre sky at ν = 100, 143, 217, 353, 545, and 857 GHz. We have chosen ν = 353 GHz as our reference frequency. At higher frequencies, the galactic dust will become more of a nuisance and at lower frequencies the CMB primary anisotropies will tend to dominate.

Frequency [GHz]	100	143	217	353	545	857
$FWHM$ [']	9.5	7.1	5.0	5.0	5.0	5.0
s_X [μKs$^{1/2}$]	32.0	21.0	32.3	99.0	990	45125

Table 1. Parameters of the PLANCK HFI detector properties, The Planck collaboration (2005)

In order to test the detectability of the dust with Planck, we evaluate the total error on $\ell(\ell+1)C_l/2\pi$:

$$\sigma = \sigma_\ell^{CMB} + \sigma_\ell^{instr} = \sqrt{\frac{2}{(2\ell+1)f_{cut}L}} \times (E_{CMB} + E_{instr}), \quad (7)$$

where f_{cut} = 0.8 is the fraction of the sky used, L is the bin-size, $E_{CMB} = \ell(\ell+1)C_\ell^{CMB}/2\pi$, Lambda web-site: http://lambda.gsfc.nasa.gov (1 March 2005), is the cosmic variance and the instrument error is

$$E_{instr} = f_{sky}\frac{4\pi s_X^2}{t_{obs}} \cdot e^{\ell^2\cdot\sigma_b^2} \cdot \frac{\ell(\ell+1)}{2\pi}, \quad (8)$$

where f_{sky} = 1 is the fraction of the sky covered, s_X is the noise [μKs$^{1/2}$], $t_{obs} = 14\cdot30\cdot24\cdot3600$ s is the observation time (14 months), and $\sigma_b = FWHM/2.35$ (FWHM is the full width at half maximum of the beam in radians).

For Planck, the values of these parameters are given in Tab. 1.

The resulting errors for a binning of L = 500 along with the dust power spectrum is plotted in Figs. 4-5. In Fig. 4, the frequency ν = 353 GHz is fixed while ℓ is varied. We note that $\ell \sim 1000$ seems to be a good place to search for dust. At low ℓ, the error due to the cosmic variance dominates, at high ℓ the instrument noise.

In Fig. 5, the ℓ multipole binning center is fixed and we show the electromagnetic spectrum of the primordial anisotropies and the early dust emission. The fourth point in the figures correspond to ν = 353 GHz and gives the best signal over noise ratio. At low ℓ the cosmic variance is important, at high ℓ, the instrument noise.

Early dust may thus produce a measurable disturbance to the primordial anisotropy angular power spectrum at high multipoles (in the Silk's damping wing). Although the primary contaminant to the CMB in the submillimeter domain is the interstellar dust emission, this new component vindicates the use of more than 2 frequencies to disentangle CMB anisotropies from submillimetre foregrounds.

Component separation methods using the full range of Planck frequencies should be able to disentangle the CMB anisotropies from early dust, far-infrared background fluctuations, and galactic dust emission.

4.2. Detection with other instruments?

There are several other instruments that might be used to detect the early dust: ALMA, Wootten (2003), BLAST, Devlin (2001), BOLOCAM (LMT) and (CSO), Mauskopf et al. (2000), MAMBO, Greve et al. (2004) and SCUBA Borys et al. (1999) and SCUBA2 Audley et al. (2004).

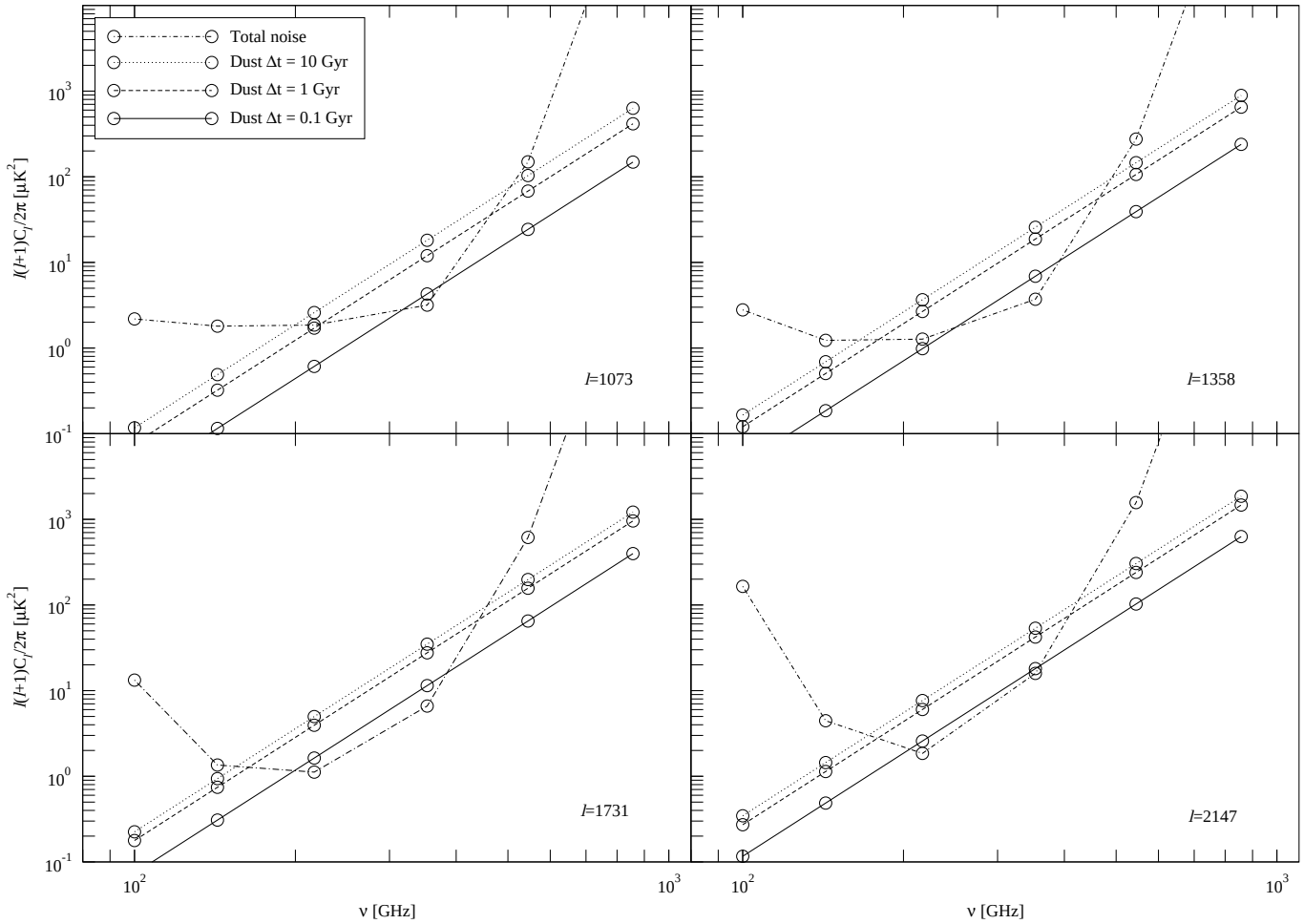

Fig. 5. Comparison between dust power spectrum and Planck error limits at ℓ=1073, 1358, 1731, and 2110 with binning 500. The error limits (total noise) consist of two parts; the CMB cosmic variance, which is constant at such μK-levels and the instrument noise has the shape of an exponential$\times\ell^2$.

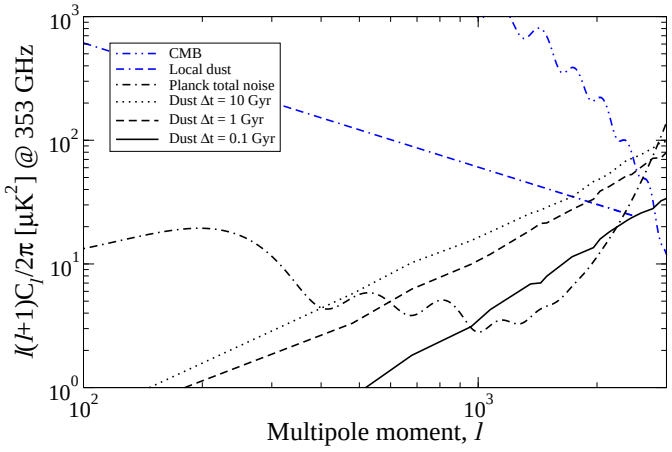

Fig. 4. Comparison between dust power spectrum, the Planck error limits and local dust (T=17 K) at 353 GHz with binning 500. The error limits (total noise) consist of two parts; the CMB cosmic variance, which dominates for small ℓ and the instrument noise, which dominates for high ℓ.

Using Eqs. 7 and 8 we have estimated the sensibilities of these detectors. The result is presented in Tab. 2. Since all these instruments operate on a small patch in the sky we use $f_{sky} = f_{cut} = 10 \cdot FOV$. The integration time has been set to one hour and the noise per second, s_X, has been calculated as $s_X = NEFD/\sqrt{N_{det}}$. The error has been evaluated at the multipole moment $\ell \sim 1/FWHM$ (for BOLOCAM(LMT) ℓ has been set to 20,000) and we have used a bin-size of $L = \ell$. The resulting sensitivities σ_ℓ^{instr} can be compared with the dust signal as plotted in Fig. 6. As can be seen, BLAST, SCUBA and MAMBO are quite out of the question for detecting the dust signal. However, BOLOCAM(LMT), ALMA and SCUBA2 have good chances of detecting the radiation from the first dust. BOLOCAM(CSO) might also be used for certain ranges of ℓ. We also note that the curves are very near parabolic. In fact, for $1,000 \lesssim \ell \lesssim 100,000$ the curves can be fitted within $\sim 10\%$ as:

$$\begin{aligned} \ell(\ell+1)C_\ell^{Dust}/2\pi &\approx 2.13\times10^{-5}\times\ell^{1.92}, \quad \Delta t = 10\ \text{Gyr}, \\ \ell(\ell+1)C_\ell^{Dust}/2\pi &\approx 1.37\times10^{-5}\times\ell^{1.95}, \quad \Delta t = 1\ \text{Gyr}, \\ \ell(\ell+1)C_\ell^{Dust}/2\pi &\approx 4.02\times10^{-5}\times\ell^{1.98}, \quad \Delta t = 0.1\ \text{Gyr}. \end{aligned} \tag{9}$$

The dependancy in ℓ, which is slightly different from an uncorrelated noise ℓ^2 behavior, means that large-scale

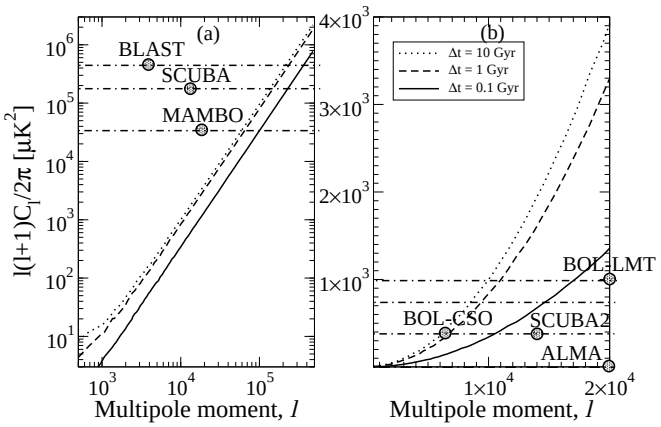

Fig. 6. Dust power spectrum as a function of multipole moment, ℓ, for different dust lifetimes. The left graph has logarithmic scales and covers the multipole region $500 \leq \ell \leq 500,000$. The right graph has linear scales and covers the multipole region $500 \leq \ell \leq 20,000$. Estimated detection limits for different instruments are also included as dotted lines with $\ell \sim 1/FWHM$ marked with a small circle.

correlations cannot be neglected. They mix differently at different epochs depending on the dust lifetime parameter.

Instrument	$NEFD$ $\left[\frac{\text{mJy}}{\sqrt{\text{Hz}}}\right]$	ν [GHz]	N_{det}	$FWHM$ ["]	FOV ['^{2}]	ℓ [10^3]	σ_ℓ^{instr} [$10^3 \mu$K^2]
SCUBA	75	353	37	13.8	4.2	14	161
SCUBA2	25	353	5120	14.5	50	14	1.8
MAMBO	30	250	117	10.7	13	19	22
BLAST	239	600	43	59	85	3.5	424
BOLOCAM							
(CSO)	40	280	144	31	50	6.6	0.38
(LMT)	3	280	144	6	3.1	20	1.0
ALMA	1.5	353	1	13.8/2	0.09	24	8.0

Table 2. Sensitivities, σ_ℓ^{instr}, for different (current and future) detectors. $NEFD$ = Noise Equivalent Flux Density, ν is the operating instrument frequency, N_{det} = Number of detectors, $FWHM$ = Full Width Half Max, FOV = Field of View in units of arcmin^2, $\ell = 1/FWHM$, E_ℓ^{instr} is the instrument error in units of mK$^2_{\text{CMB}}$. The instrument sensitivity, has been calculated with Eqs. 7, 8 using t_{obs} = 1h, $f_{sky} = f_{cut} = 10 \cdot FOV$ and $L = \ell$.

5. Conclusions

There seems to be a possibility to detect the dust from the first generation of stars with the Planck satellite on small angular scales ($\ell \gtrsim 1000$).

However, the detectability depends on the actual distribution of dust in the early universe, but also to a large extent on the dust lifetime.

The results are parametrized so that changing the frequency and the fraction of produced metals that become dust is only a matter of scaling the figures: $C_\ell \propto (\nu/353\,\text{GHz})^4$ and $C_\ell \propto (f_d/0.3)^2$. The spectrum of the early dust is compared to that of the primary CMB anisotropies as well as local dust.The unique spectral signature of the early dust will help in disentangling it from the CMB and the different foregrounds (local dust and extragalactic far infrared background).

The spatial signature of the early dust is found to have $C_\ell \approx$ constant $\approx 10^{-4}\,\mu\text{K}^2_{CMB}$. Obviously, other signals that are correlated with the structures will also show a similar behavior in the power spectrum. Notably the near infrared background from primordial galaxies could be correlated with the early dust.

The next generation of submm instruments will be adequate to measure these early dust anisotropies at very small angular scales ($\ell \gtrsim 2000$). Our estimation shows that BOLOCAM, SCUBA2 and ALMA have a good prospect of finding the early dust. However, for these instruments, more detailed simulations are required in order to obtain a realistic dark matter and baryon distribution. A DM simulation on a smaller box, maybe $L = 50h^{-1}$ for PLANCK, smaller still for ALMA, would improve the results on the relevant angular scales $z \gtrsim 1000$. This also means that the particles are smaller, giving a better level of detail. Furthermore, the distribution of dust relative the dark matter can also be improved and it is even possible to include some semi-analytical results from the galaxy simulations in GalICS.

References

Audley, M. D., Holland, W. S., Hodson, T., et al. 2004, in Astronomical Structures and Mechanisms Technology. Edited by Antebi, Joseph; Lemke, Dietrich. Proceedings of the SPIE, Volume 5498, pp. 63-77 (2004)., ed. J. Zmuidzinas, W. S. Holland, & S. Withington, 63–77

Bennett, C. L., Halpern, M., Hinshaw, G., et al. 2003, ApJS, 148, 1

Blaizot, J., Guiderdoni, B., Devriendt, J. E. G., et al. 2004, MNRAS, 352, 571

Blaizot, J., Szapudi, I., Colombi, S., et al. 2006, MNRAS, 369, 1009

Blaizot, J., Wadadekar, Y., Guiderdoni, B., et al. 2005, MNRAS, 360, 159

Borys, C., Chapman, S. C., & Scott, D. 1999, MNRAS, 308, 527

Boulanger, F., Abergel, A., Bernard, J.-P., et al. 1996, A&A, 312, 256

Cattaneo, A., Blaizot, J., Devriendt, J., & Guiderdoni, B. 2005, MNRAS, 364, 407

Cen, R. 2003, ApJL, 591, L5

Colless, M., Dalton, G., Maddox, S., et al. 2001, MNRAS, 328, 1039

Devlin, M. 2001, in Deep Millimeter Surveys: Implications for Galaxy Formation and Evolution, 59–66

Draine, B. T. 1990, in ASP Conf. Ser. 12: The Evolution of the Interstellar Medium, 193–205

Efstathiou, G. 2003, MNRAS, 343, L95

Eke, V. R., Cole, S., & Frenk, C. S. 1996, MNRAS, 282, 263
Elfgren, E. & Désert, F.-X. 2004, A&A, 425, 9
Greve, T. R., Ivison, R. J., Bertoldi, F., et al. 2004, MNRAS, 354, 779
Hannestad, S. 2003, Journal of Cosmology and Astro-Particle Physics, 5, 4
Hatton, S., Devriendt, J. E. G., Ninin, S., et al. 2003, MNRAS, 343, 75
Komatsu, E., Kogut, A., Nolta, M. R., et al. 2003, ApJS, 148, 119
Lambda web-site: http://lambda.gsfc.nasa.gov. 1 March 2005
Mauskopf, P. D., Gerecht, E., & Rownd, B. K. 2000, in ASP Conf. Ser. 217: Imaging at Radio through Submillimeter Wavelengths, ed. J. G. Mangum & S. J. E. Radford, 115–+
Ninin, S. 1999, PhD thesis: Université Paris 11
Oh, S. P., Cooray, A., & Kamionkowski, M. 2003, MNRAS, 342, L20
Spergel, D. N., Verde, L., Peiris, H. V., et al. 2003, ApJS, 148, 175
Subramanian, K., Seshadri, T. R., & Barrow, J. D. 2003, MNRAS, 344, L31
Szapudi, I., Bond, J. R., Colombi, S., et al. 2001, in Mining the Sky, 249
The Planck collaboration. 2005, Available at: http://www.rssd.esa.int/SA/PLANCK/docs/Bluebook-ESA-SCI(2005)1.pdf
Wootten, A. 2003, in Large Ground-based Telescopes. Edited by Oschmann, Jacobus M.; Stepp, Larry M. Proceedings of the SPIE, Volume 4837, pp. 110-118 (2003)., 110–118